Medical Microbiology and Immunology (2024) 213:26
https://doi.org/10.1007/s00430-024-00807-x

RESEARCH

Inhibiting lipid droplet biogenesis enhances host protection against hypervirulent *Klebsiella pneumoniae* infections

Hui-Jung Jung[1] · Hyun Ah Kim[2] · Miri Hyun[2] · Ji Yeon Lee[2] · Young Jae Kim[3,4,5] · Seong-Il Suh[1] · Eun-Kyeong Jo[3,4,5] · Won-Ki Baek[1] · Jin Kyung Kim[1]

Received: 2 April 2024 / Accepted: 18 October 2024 / Published online: 14 November 2024

Abstract

Hypervirulent *Klebsiella pneumoniae* (hvKp), an emerging Kp subtype, has become a serious global pathogen. However, the information regarding host interactions and innate immune responses during hvKp infection is limited. Here, we found that hvKp clinical strains increased triacylglycerol synthesis, resulting in lipid droplets (LDs) formation via the mammalian target of rapamycin signaling pathway in RAW264.7 cells. Treatment with rapamycin, an inhibitor of this pathway, affected LDs formation and antimicrobial responses against clinical hvKp infections. In accordance with the role of LDs in modulating inflammation, the pharmacological inhibition of lipogenesis reduced proinflammatory cytokine expression during hvKp infections. In addition, inhibition of LDs formation using pharmacological inhibitors and knockdown of lipogenesis regulators decreased the intracellular survival of hvKp in macrophages. Moreover, inhibiting LDs biogenesis reduced mortality, weight loss, and bacterial loads in hvKp-infected mice. Collectively, these data suggest that LDs biogenesis is crucial in linking host immune responses to clinical hvKp infections.

Keywords Hypervirulent · *Klebsiella pneumoniae* · Macrophages · Lipid droplets · mTOR

Introduction

Classical *Klebsiella pneumoniae* (cKp) is a Gram-negative, opportunistic bacterium that causes various infections, including pneumonia, bloodstream infections, and meningitis in immunocompromised patients [1]. However, in recent decades, a more virulent subtype of Kp, known as hypervirulent Kp (hvKp), has emerged as a significant global pathogen. First identified in Taiwan, hvKp is now responsible for a wide range of severe infections, including liver abscesses, pneumonia, and meningitis, even in healthy individuals [2, 3]. Unlike cKp, hvKp possesses several enhanced virulence factors, including a hypermucoviscous phenotype, which allows it to evade host immune responses more effectively [4].

The hypermucoviscous phenotype of hvKp is regulated by genes such as *rmpA* and *rmpA2*, which enable the bacterium to produce a thick capsule, providing protection against phagocytosis by neutrophils and macrophages [5]. Additionally, hvKp expresses high-affinity iron acquisition systems like aerobactin, which enhances bacterial survival in iron-limited environments within the host [6]. These

Hui-Jung Jung and Hyun Ah Kim contributed equally to this work.

✉ Won-Ki Baek
wonki@dsmc.or.kr

✉ Jin Kyung Kim
pcjlovesh6@kmu.ac.kr

1 Department of Microbiology, Keimyung University School of Medicine, Daegu 42601, Korea

2 Department of Infectious Diseases, Keimyung University Dongsan Hospital, Keimyung University School of Medicine, Daegu 42601, Korea

3 Department of Microbiology, Chungnam National University College of Medicine, Daejeon 35015, Korea

4 Infection Control Convergence Research Center, Chungnam National University College of Medicine, Daejeon 35015, Korea

5 Department of Medical Science, Chungnam National University College of Medicine, Daejeon 35015, Korea

virulence mechanisms allow hvKp to survive intracellularly in macrophages, further contributing to its pathogenicity [7].

Another critical difference between hvKp and cKp is their epidemiology. While cKp typically causes hospital-acquired infections, hvKp is responsible for community-acquired infections, often in otherwise healthy individuals [8]. Additionally, hvKp, which was originally associated with good antibiotic susceptibility and primarily caused infections in healthy individuals within the community, has recently shown increasing rates of antibiotic resistance, raising global concerns [9]. Therefore, understanding immunomodulation during hvKp infections in immune cells is necessary.

Traditionally, lipid droplets (LDs) were recognized primarily as cellular storage organelles for neutral lipids such as triglycerides (TGs) and cholesterol esters, especially in adipocytes [10]. However, recent research has elucidated their pivotal roles in inflammatory responses and metabolic processes within myeloid cells, including macrophages [11]. In macrophages, LDs mediate inflammatory responses via eicosanoid production, which contribute to inflammation, innate immune responses, and cell growth [12]. In particular, *Mycobacterium tuberculosis* (Mtb) infection induce the formation of LDs-laden macrophages within tuberculous granulomas, which are termed as foamy macrophages [13]. As Mtb-infected foamy macrophages contribute to dissemination and granuloma development, controlling foamy macrophage formation during Mtb infections is important [13]. During a *Streptococcus uberis* infection, foamy macrophages are induced through fatty acid-binding protein 4, and play important roles in inflammation and host defense [14]. Additionally, internalized *Salmonella* Typhimurium has been found to increase LDs biogenesis in murine macrophages; the pharmacological modulation of LDs formation has shown altered bacterial proliferation [15]. Although there is a report that Kp infection promotes LDs formation in human monocytes [16], the mechanisms by which LDs are generated and the roles of the formed LDs during Kp infection have not been studied.

The mammalian target of rapamycin (mTOR) signaling pathway is a molecular mechanism involved in LDs formation. The conditioned medium from murine adipose-derived mesenchymal stromal cells promote LDs biogenesis mTOR/peroxisome proliferator-activated receptor (PPAR) signaling in macrophages [17]. During intracellular parasite *Toxoplasma gondii* infections, c-Jun kinase and mTOR signaling are necessary for LDs generation in human foreskin fibroblasts [18]. Furthermore, mTOR regulates the expression of sterol regulatory element-binding protein, a transcription factor for lipid metabolism-related genes, via controlling lipin 1 localization [19].

In this study, we identified the critical roles and molecular mechanisms underlying LDs formation in hvKp-infected macrophages. Three clinical strains of hvKp induced LDs formation and regulated lipid metabolism. We confirmed that LDs are formed through the mTOR signaling pathway and that rapamycin, an inhibitor of mTOR, regulates LDs formation, lipid metabolism, and antimicrobial responses during hvKp infections. We further showed that pharmacological inhibitors of lipogenesis regulate proinflammatory cytokine production and enhance antimicrobial responses, suggesting the involvement of LDs in the intracellular survival of hvKp in macrophages. Moreover, the suppression of LDs biogenesis has broader implications for in vivo hvKp infections. Inhibiting LDs formation decreased bacterial loads and host susceptibility to hvKp infection in mice. The novelty of suppressing LDs biogenesis lies in its dual impact; that is, it controls a critical component of the host's inflammatory response while simultaneously undermining the intracellular survival mechanisms of hvKp. This approach represents a significant advancement in our understanding of host-pathogen interactions.

Materials and methods

Cell culture

The murine macrophage cell lines RAW264.7 (TIB-71, American Type Culture Collection) were maintained in the Dulbecco's Modified Eagle's Medium (DMEM; Welgene, Gyeonsan, Korea), supplemented with 10% fetal bovine serum (Welgene) and 1% penicillin/streptomycin (Gibco BRL, Grand Island, NY, USA). Cells were incubated in a humidified atmosphere at 37 °C with 5% CO_2.

Bacterial strains and culture

Sixteen Kp isolates were obtained from the various clinical specimens of Keimyung University Dongsan Hospital. From these strains, we collected the three hvKp strains (DSMC-K210, DSMC-K285, DSMC-K360) from blood specimens of patients with a liver abscess. These isolates were identified using the automated microbial identification and susceptibility test system (VITEK 2 system, bioMerieux, Lyon, France). Extended-spectrum β-lactamase (ESBL) production was confirmed by agar dilution test using cefotaxime and ceftazidime along with clavulanate, in accordance with the Clinical and Laboratory Standards Institute guidelines [20]. Capsular serotypes and genes of virulence factors were identified by polymerase chain reaction (PCR) [6, 21]. Strains were serotyped as: K1, K2, K5, K20, K54, and K57, or as non-determining when no specific serotype could be

identified. Hypervirulent characteristics were confirmed with a string test and gene amplification of *rmpA*, *magA*, and aerobactin. According to serotype analysis, the three hvKp isolates were of the K1 serotype. HvKp had antibiotic susceptibility for most antibiotics except ampicillin.

Strains of Kp were grown in Luria-Bertani (LB) broth (Difco, Becton Dickinson, Sparks, MD, USA) for liquid culture and on LB agar (Difco) as a solid medium at 37 °C. All bacteria were stored at -80 °C in LB broth supplemented with 15% v/v glycerol (Sigma-Aldrich, St. Louis, MO, USA). For infection stocks, bacteria were incubated overnight and then diluted in fresh LB broth and cultured to an optical density (OD 600 nm) of 0.1. Samples were frozen at -80 °C with 15% glycerol, and one aliquot was counted prior to infection.

Infection and treatments

RAW264.7 cells were replated into 6-well or 24-well plates in complete DMEM medium at a density of 7×10^5 cells/well and infected with the different strains at multiplicity of infection (MOI) of 40 for 1 h. After that, cells were washed three times with PBS and incubated for an additional 1 h in a medium containing 300 µg/ml gentamicin (15710-072, Gibco) and 15 µg/ml polymyxin B (81271, Sigma-Aldrich) to remove non-phagocytosed bacteria. After incubation, media were removed again, and fresh media was added for the remainder of the experiment time. To inhibit the mTOR signaling pathway, 200 nM of rapamycin (553210, Sigma-Aldrich) was added to the cell culture and incubated for 30 min prior to hvKp infection. To impair the LDs biogenesis, 10 µM of diacylglycerol O-acyltransferase 1 (DGAT1) inhibitor (A922500, A1737, Sigma-Aldrich) or 15 nM of cytosolic phospholipase A_2 ($cPLA_2$) inhibitor (CAY10650, 10743, Cayman Chemical, Michigan, USA) were added to the cell culture and incubated for 1 h before hvKp infection, and this remained for the entire infection time, at 37 °C in 5% CO_2. The inhibitors were dissolved in dimethyl sulfoxide (DMSO, 20–139, Sigma-Aldrich).

Cell proliferation assay

The rate of cell proliferation was evaluated using CellTiter 96® AQueous One Solution Cell Proliferation Assay (G3580, Promega, Madison, WI, USA). In brief, cells were seeded in a 96-well plate at a density of 3×10^4 cells per well. The cells were incubated at 37 °C in a 5% CO_2 incubator for 18 h. Treatment of A922500 or CAY10650 were applied and incubated for 24 h. Subsequently, the cells were incubated with 20 µL of CellTiter 96® AQueous One Solution reagent for an additional 30 min. The absorbance was measured using a Synergy/HTX spectrophotometer (BioTek instrument, Inc. Winooski, VT, USA). All the readings were normalized to the control, and the control was considered as 100% live cells. An average of three experiments was performed.

Immunoblotting

Cells were lysed in RIPA lysis buffer (89900, Thermo Scientific™, Waltham, MA, USA) and supernatant fractions were collected. Protein concentrations were measured with bicinchoninic acid (Pierce, Rockford, IL, USA), and equal amounts of proteins (50 µg/lane) were separated by 8% sodium dodecyl-sulfate polyacrylamide gel electrophoresis and transferred to the nitrocellulose membranes (GE Healthcare Life Science, Pittsburgh, PA, USA) incubated with a specific antibody. The anti- fatty acid synthase (FAS, #3180, Cell Signaling Technology, Beverly, MA, USA), anti-perilipin 1 (PLIN1, NB100-449, Novus Biologicals, Centennial, CO, USA), anti-acetyl-CoA carboxylase 2 (ACC2, #3676, Cell Signaling Technology), anti- phospho- ACC2 (Ser79) (#3661, Cell Signaling Technology), anti- ACC1 (#4190, Cell Signaling Technology), anti-stearoyl-CoA desaturase-1 (SCD1, #2794, Cell Signaling Technology), anti-phospho-mTOR (Ser2448) (#2971, Cell Signaling Technology), anti-phospho-p70S6K (Thr421/Ser424) (#9204, Cell Signaling Technology), and phospho-S6 Ribosomal Protein (Ser235/236) (#2211, Cell Signaling Technology), anti-DGAT1 (#NB110-41487, Novus Biologicals) and anti-$cPLA_2$ (#sc-454, Santa Cruz Biotechnology, Inc.) were used as primary antibodies. These antibodies were used at a dilution of 1:1,000. The anti-ACTB antibody (A5441) was acquired from Sigma-Aldrich (Merck KGaA) and used at a dilution of 1:5000. Secondary antibodies (anti-rabbit IgG [1:5,000 diluted; 111-035-045] and anti-mouse IgG [1: 5,000 diluted; 115-035-062]) were purchased from Jackson ImmunoResearch Laboratories, Inc. (West Grove, PA, USA). Bands were detected using the Immobilon Western Chemiluminescent HRP Substrate (EMD Millipore, Darmstadt, Germany).

RNA isolation and quantitative real-time polymerase chain reaction (qRT-PCR)

Total RNA was extracted from infected cells and the lung, liver, and spleen tissues using TRIzol (15596-026, Thermo Fisher Scientific, Waltham, MA, USA), following the manufacturer's instructions. Then, RNA was reverse transcribed to complementary DNA using the reverse transcriptase premix (EBT-1515, Elpis Biotech, Daejeon, Korea). Data were analyzed by the qTOWER3 PCR thermal cycler (Analytik Jena, Jena, Germany) using the THUNDERBIRD SYBR qPCR Mix (QPS-201, TOYOBO, Osaka, Japan). The gene

expression was calculated using the $2^{\Delta\Delta}$ threshold cycle (Ct) method and normalized to *b-actin*. The primer sequences (mouse) were as follows: *Il6* forward: 5'- ACAAAGCCA GAGTCCTTCAGA-3', reverse: 5'- TGGTCCTTAGCCA CTCCTTC-3'; *Tnfa* forward: 5'- CCCACGTCGTAGCA AACCAC-3', reverse: 5'- GCAGCCTTGTCCCTTGAAG A-3'; *Agpat2* forward: 5'-AGCGGACAGAAGAAACTG GAGG-3', reverse: 5'- TTAGCTCACGCTTGGCGATCT G-3'; *Dgat2* forward: 5'- CTGTGCTCTACTTCACCTGG CT-3', reverse: 5'-CTGGATGGGAAAGTAGTCTCGG-3'; *Acaca* forward: 5'-GATATCCCAGAGATGTTTCGGC-3', reverse: 5'- GTCAGCATGTCAGAAGGCAGAG-3'; *Scd1* forward: 5'-CCGAAGTCCACGCTCGAT- 3', reverse: 5'-TGGAGATCTCTTGGAGCATGTG-3'; *Fasn* forward: 5'-CACAGTGCTCAAAGGACATGCC-3', reverse: 5' - CAC CAGGTGTAGTGCCTTCCTC −3'; and *b-actin* forward: 5'-CCACCATGTACCCAGGCATT-3', reverse: 5'-AGGG TGTAAAACGCAGCTCA-3'.

Small interfering RNA transfection

For transient silencing of DGAT1 and $cPLA_2$ in RAW264.7 murine macrophage cells, DGAT1 siRNA (#sc-40488), $cPLA_2$ siRNA (#sc-35098), and a scrambled siRNA (#sc-37007) were obtained from Santa Cruz Biotechnology, Inc. All siRNAs were transfected using Lipofectamine® 2000 Reagent (11668027, Invitrogen, Carlsbad, CA, USA). RAW264.7 cells were seeded in 24-well plates at a density of 20×10^4 cells per well and transfected with the 200 nM siRNAs using Lipofectamine® 2000. After transfection at 4 h, the medium was changed to growth medium, and then transfected cells were infected with hvKp strains for 4–6 h. The cells were then harvested for ELISA measurements and CFU analysis.

Colony forming units (CFUs) assay from macrophage and mice organs

RAW264.7 cells were infected with hvKp at a MOI of 40 for 1 h at 37 °C, 5% CO_2 in an antibiotic-free medium. After that, the cells were washed three times with PBS and incubated for an additional 1 h in a medium containing 300 μg/ml gentamicin and 15 μg/ml polymyxin B. Then, cells were washed and subsequently lysed with 1% saponins in PBS. 10-fold serial dilutions of the lysate were plated on LB agar plates incubating overnight at 37 °C to determine the number of CFUs. The lungs, livers, and spleens were harvested, homogenized in PBS, serially diluted in PBS, and plated on LB agar. Colonies formed in the plates were counted after 24 h of incubation.

Enzyme-linked immunosorbent assay (ELISA)

RAW264.7 cells were cultured in 24-well culture plates at a density of 2×10^5 cells per well. Media were collected after overnight culture and centrifuged at 2000 × *g* for 5 min at 4 °C to remove cell debris. Culture supernatants and mice organ extracts (the lung, liver, and spleen) were assayed for TNF-α using the mouse TNF-alpha Quantikine ELISA Kit from R&D Systems (MTA00B, Minneapolis, MN, USA) according to the manufacturer's instructions.

Immunofluorescence and analysis

For LDs quantification, infected cells were fixed with 4% paraformaldehyde for 15 min and then permeabilized with 0.25% Triton X-100 (Sigma-Aldrich) for 10 min. Next, cells were incubated with BODIPY 493/503 (D3922, Molecular Probes, Eugene, OR, USA), according to the manufacturer's instructions. Nuclei were stained with 4′,6-diamidino-2-phenylindole (D9542, Sigma-Aldrich) for 5 min at room temperature. Immunofluorescence images were observed and analyzed using the confocal laser microscope (TCS SP8, Leica Microsystems, Wetzlar, Germany) and Image J software (National Institutes of Health, Bethesda, MD, USA).

To verify the LDs volume and mass after hvKp infection, subcultured macrophages in a glass-bottom TomoDish were treated with hvKp for 1 h. After washing with PBS (and with gentamicin), the cells in each group were incubated for an additional 4 h in a medium. All experiments were performed in a TomoChamber (Tomocube, Daejeon, Korea) maintained at 37 °C using humidified 5% CO_2. Based on the results of RI distribution in a single cell ($n = 5$/group), the quantitative changes of LDs volume and mass in each group were determined and monitored.

Triglycerides (TGs) level measurements

According to the manufacturer's instructions, levels of TGs in macrophages lysate were measured using EZ-Triglyceride Quantification Assay kits (DG-TGC100, DoGenBio, Seoul, Korea). Briefly, RAW264.7 cells were cultured and infected with hvKp. Then, the cell lysates (50 μl) for each sample were transferred into a 96-well plate and incubated with the triglyceride reaction mixture (50 μl) at room temperature for 30 min in a dark room. TGs levels in the cells were determined by measuring the Fluorometric (535 nm / 595 nm) using the Synergy/HTX (BioTek instrument, Inc).

Animal experiments

In this study, wild-type male C57BL/6 mice at 8–9 weeks old were purchased from Samtako BioKorea Co. (Osan, Korea). Mice were kept in a specific pathogen-free environment with a 12-h light/dark cycle at 23–25 °C and humidity of 35-75% and received enriched water and ad libitum feeding. All mice were adapted to this environment for 1 week. The mice were randomly assigned to three groups: the PBS control group, hvKp group, and combined treatment group with A922500 + hvKp, each consisting of five mice. For in vivo experiments, mice were infected with an i.p. or i.n. administration of hvKp suspension (1×10^3 CFU suspended in 1 ml or 25 µl sterile PBS), respectively. Treatment with A922500 was administered i.p. at a dose of 3 mg/kg/day, starting one day before infection. The same dose was given once daily for the remaining days throughout the experiment. Control mice were i.p. administered with an equal volume of sterile PBS. Mice were sacrificed 24 h after hvKp injection to harvest organs. The lung, liver, and spleen tissues were homogenized and used for RNA, ELISA, and CFU preparation. All animals were maintained under barrier conditions in a biohazard animal room at the School of Medicine, Keimyung University, Daegu, Korea.

Survival analysis

Mice (5 mice in each group) were treated as described above and closely monitored every day. Survival and body weight rates were measured continuously for 7 days in each group and recorded every 24 h.

Histology

For histopathology, lungs, livers, and spleens from hvKp group or A922500 + hvKp group mice (4 mice in each group) were harvested after 48 h. Tissue samples were fixed in 10% formalin and then they were embedded in paraffin wax. Paraffin sections of 4 µm thickness were cut and were stained with hematoxylin and eosin for light microscopic examination. Whole fields of tissue were scanned to determine the inflamed areas in the lungs and white pulp areas per red pulp in the spleens from each mouse. The number of neutrophils per 0.16 mm^2 in the livers from each mouse was counted across eight sections with every eight views to obtain a semi-quantitative estimation.

Ethics statements

This study was approved by the Institutional Research and Ethics Committee at Keimyung University School of Medicine (approval number: KM-2023-22R1) and Chungnam National University College of Medicine (approval number: 202109 A-CNU-180). All animal experiments were performed in accordance with the guidelines of the Korean Food and Drug Administration.

Statistical analysis

Data are presented as mean ± standard deviation and were obtained from three independent experiments. The Student t-test or analysis of variance was used to analyze the data. Statistical analyses were performed, and graphs were made using GraphPad Prism 7.0 software for Windows (GraphPad Software Inc., La Jolla, CA, USA). *P*-values < 0.05, 0.01, and 0.001 were considered statistically significant.

Results

Infection with hvKp promotes LDs formation in macrophages

To determine the association between LDs formation and hvKp infection, three clinical hvKp strains were isolated from blood and pus samples, as shown in Table S1. We first analyzed LDs formation in RAW264.7 cells using the fluorescent dye BODIPY493/503. Three clinical hvKp strains induced LDs formation in RAW264.7 cells (Fig. 1A). Additionally, hvKp infections increased the protein levels of perilipin 1 (PLIN1), an LDs protein (Fig. 1B). Confocal microscopy demonstrated significantly increased intensity of BODIPY in a MOI-dependent manner (Fig. 1C). Furthermore, we confirmed the increased number and volume of LDs in the macrophages using 3D holotomography (Fig. 1D). To further verify that hvKp increased TGs synthesis in macrophages, we examined the intracellular TGs levels and observed an increase following hvKp infections (Fig. 1E). These data indicate that the hvKp infections regulates LDs and TGs synthesis in murine macrophages.

Infection with hvKp upregulates lipid metabolism in macrophages

To elucidate the mechanism behind hvKp exploiting LDs homeostasis, we investigated the regulation of host lipid metabolism during infection. We measured the mRNA expression of 1-acylglycerol-3-phosphate O-acyltransferase 2 (*Agpat2*) and diacylglycerol acyltransferase 2 (*Dgat2*), which were involved in TGs synthesis in macrophages during infection. We observed that hvKp-infected cells showed higher mRNA expression levels of *Agpat2* and *Dgat2* compared with those of uninfected cells (Fig. 2A). Moreover, infection with DSMC-K285 and DSMC-K360

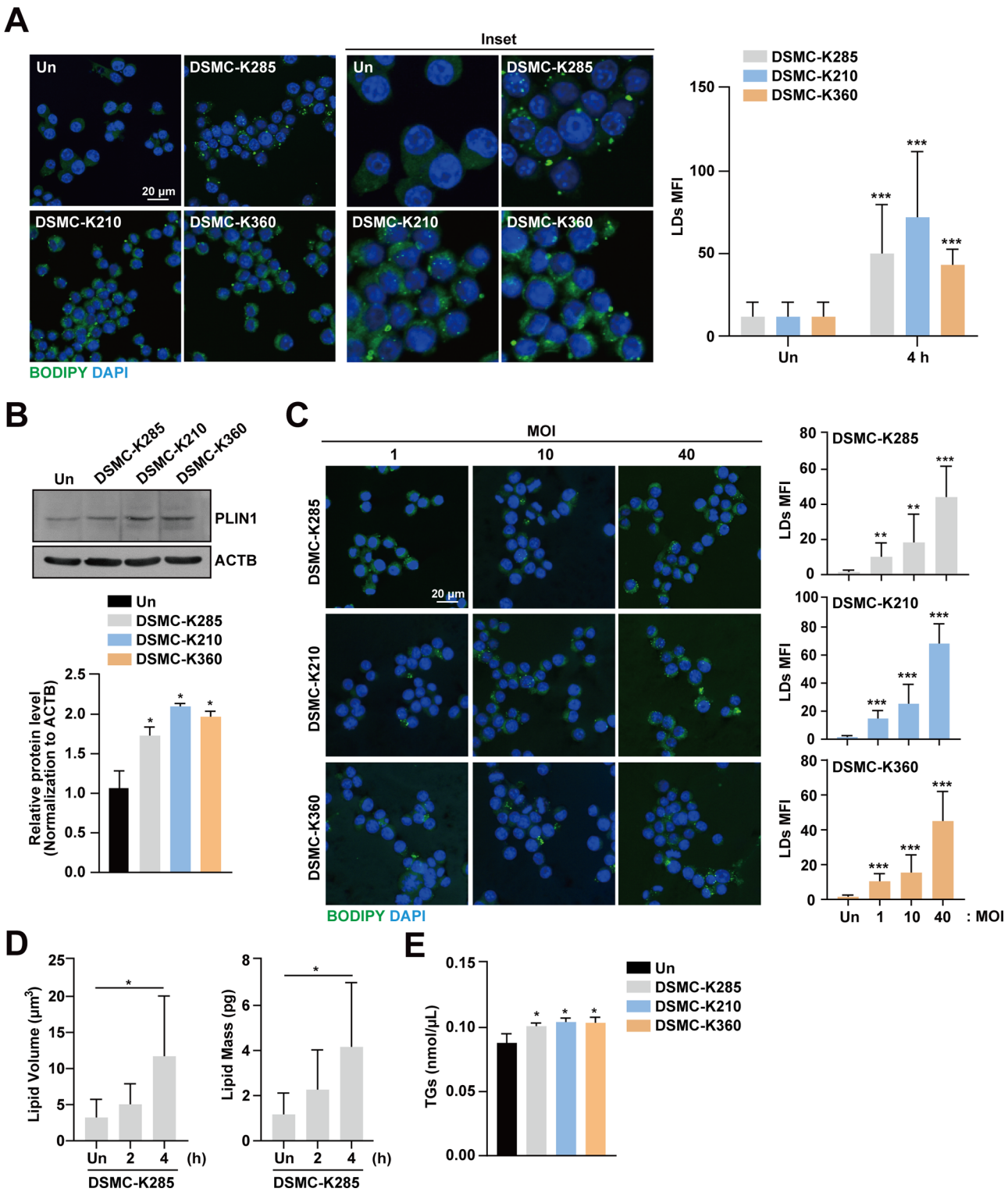

significantly increased the expression of genes related to fatty acids synthesis, including acetyl-CoA carboxylase alpha (*Acaca*), stearoyl-CoA 9-desaturase 1 (*Scd1*), and fatty acid synthase (*Fasn*) (Fig. 2B). During the DSMC-K210 infection, only the *Fasn* gene was upregulated, and no changes were observed in *Acaca* and *Scd1* expressions.

We also investigated the protein expression levels of lipid metabolism-related factors. The protein expression levels of FAS, acetyl-CoA carboxylase (ACC)1, ACC2, and SCD1 significantly increased, whereas those of phospho-ACC2 decreased following hvKp infections and compared with those in uninfected cells (Fig. 2C, D; Supplementary Fig. 1).

Fig. 1 HvKp strains induce LDs formation in RAW264.7 murine macrophage cell line. **A** RAW264.7 cells were infected with hvKp strains (MOI 40) for 4 h and were stained with BODIPY 493/503 (green) and DAPI (for nuclei). Representative images were analyzed using confocal microscopy. Scale bar, 20 μm (left). Mean fluorescence intensity (MFI) of BODIPY 493/503-stained cells (right). **B** RAW264.7 cells were infected with hvKp for 1 h. Cells were lysed and subjected to immunoblotting using antibodies against PLIN1 and ACTB (upper). The relative ratio was the densitometry of total protein after normalization to ACTB (lower). **C** RAW264.7 cells were infected with hvKp at different MOI for 4 h and stained with BODIPY 493/503 (green) and DAPI (for nuclei). Images were visualized using confocal microscopy. Scale bar, 20 μm (left). MFI of BODIPY 493/503-stained cells (right). **D** RAW264.7 cells were infected with hvKp (MOI 40) for 4 h. Representative 3D rendered images of control and hvKp infections. Quantitative analysis of LDs volume (fL)/cell volume (fL) and dry mass of LDs (pg)/cell mass (pg) for each group. Each parameter is calculated from each group. **E** RAW264.7 cells were infected with hvKp strains (MOI 40) for 4 h and triglycerides (TGs) levels were measured using an enzymatic assay kit. Data are expressed as the mean ± standard deviation of the three independent experiments. Un, uninfected; LDs, lipid droplets. *$P < 0.05$, **$P < 0.01$, and ***$P < 0.001$ according to analysis of variance

These findings suggest that the hvKp infections modulate TGs and fatty acids synthesis in murine macrophages.

Involvement of the mTOR pathway in LDs formation during hvKp infections

To further investigate the specific mechanism of hvKp infection-mediated lipid metabolism regulation, we focused on the mTOR signaling pathway. Previous studies have shown that mTOR is a crucial regulator in lipid biosynthesis and metabolism [22, 23]. As shown in Fig. 3A, the hvKp infections increased the phosphorylation of mTOR and its downstream targets, p-p70S6K and p-S6. To confirm mTOR involvement in regulating LDs formation, we used the chemical inhibitor rapamycin to suppress mTOR expression. Indeed, rapamycin inhibited the formation of LDs and protein expression of phosphorylated mTOR, p70S6K, and S6 (Fig. 3B–D). Additionally, the mRNA and protein expression of lipogenesis-related markers decreased following rapamycin treatment (Fig. 3E, F). These findings suggest that mTOR signaling plays a role in mediating LDs formation and lipid synthesis in macrophages during hvKp infections.

LDs formation is associated with inflammatory responses in hvKp-infected macrophages

HvKp infection induces a cytokine storm, increasing mortality [9]; hence, regulating inflammatory responses is crucial. Moreover, several studies have indicated that LDs play dual roles—regulating lipid homeostasis and actively contributing to inflammatory responses via diverse pathways [24]. Therefore, we explored the possibility of LDs regulating inflammatory mediator expression during the hvKp infections. Our findings revealed that the hvKp infections upregulated tumor necrosis factor (*Tnf*)*a* and interleukin (*Il*)6 expression (Supplementary Fig. 2A). *Tnfa* and *Il6* expression began to increase as early as 2 h after bacterial infection. To investigate the role of LDs formation in hvKp infection-induced inflammatory responses, we pretreated RAW264.7 cells with lipogenesis inhibitors: CAY10650 (targeting $cPLA_2$) or A922500 (targeting DGAT1). Subsequently, we assessed the inflammatory responses using qRT–PCR and ELISA. We used non-cytotoxic concentrations of the lipogenesis inhibitors (Supplementary Fig. 2B). Pretreatment with A922500 or CAY10650 reduced the elevated mRNA levels of proinflammatory genes following the hvKp infections (Fig. 4A, B). Moreover, A922500 or CAY10650 treatment reduced TNF-α production in macrophages during the hvKp infections (Fig. 4C). To determine if DGAT1 and $cPLA_2$ influence cytokine production using small interfering RNA (siRNA), we assessed the knockdown efficiency by measuring protein expression (Supplementary Fig. 3). Knockdown of DGAT1 and $cPLA_2$ reduced TNF-α production in cell culture supernatant during hvKp infections (Fig. 4D). These data suggest that regulation of LDs formation and lipogenesis in host cells contributes to controlling inflammatory responses during hvKp infections.

Inhibiting lipogenesis contributes to antimicrobial responses against hvKp infections

Confocal microscopy confirmed that inhibiting $cPLA_2$ and DGAT1 suppressed hvKp infection-induced LDs formation and TGs production (Fig. 5A, B; Supplementary Fig. 4A). To explore the promotion of host-protective responses by LDs formation, macrophages were pretreated with lipogenesis inhibitors and infected with hvKp. In parallel with LDs inhibition, A922500 and CAY10650 pretreatment reduced the bacterial loads in macrophages (Fig. 5C). Lipogenesis inhibitor treatment did not affect bacterial growth (Supplementary Fig. 4B). Similar to the results with the inhibitor treatments, knockdown of DAGT1 and $cPLA_2$ reduced intracellular bacterial survival in macrophages, suggesting the potential of targeting DGAT1 and $cPLA_2$ for therapy during hvKp infection (Fig. 5D). In addition, rapamycin treatment significantly decreased the intracellular bacterial loads in macrophages (Fig. 5E). The data reveal that suppression of LDs formation and inhibition of the mTOR signaling pathway promotes antimicrobial responses during hvKp infections.

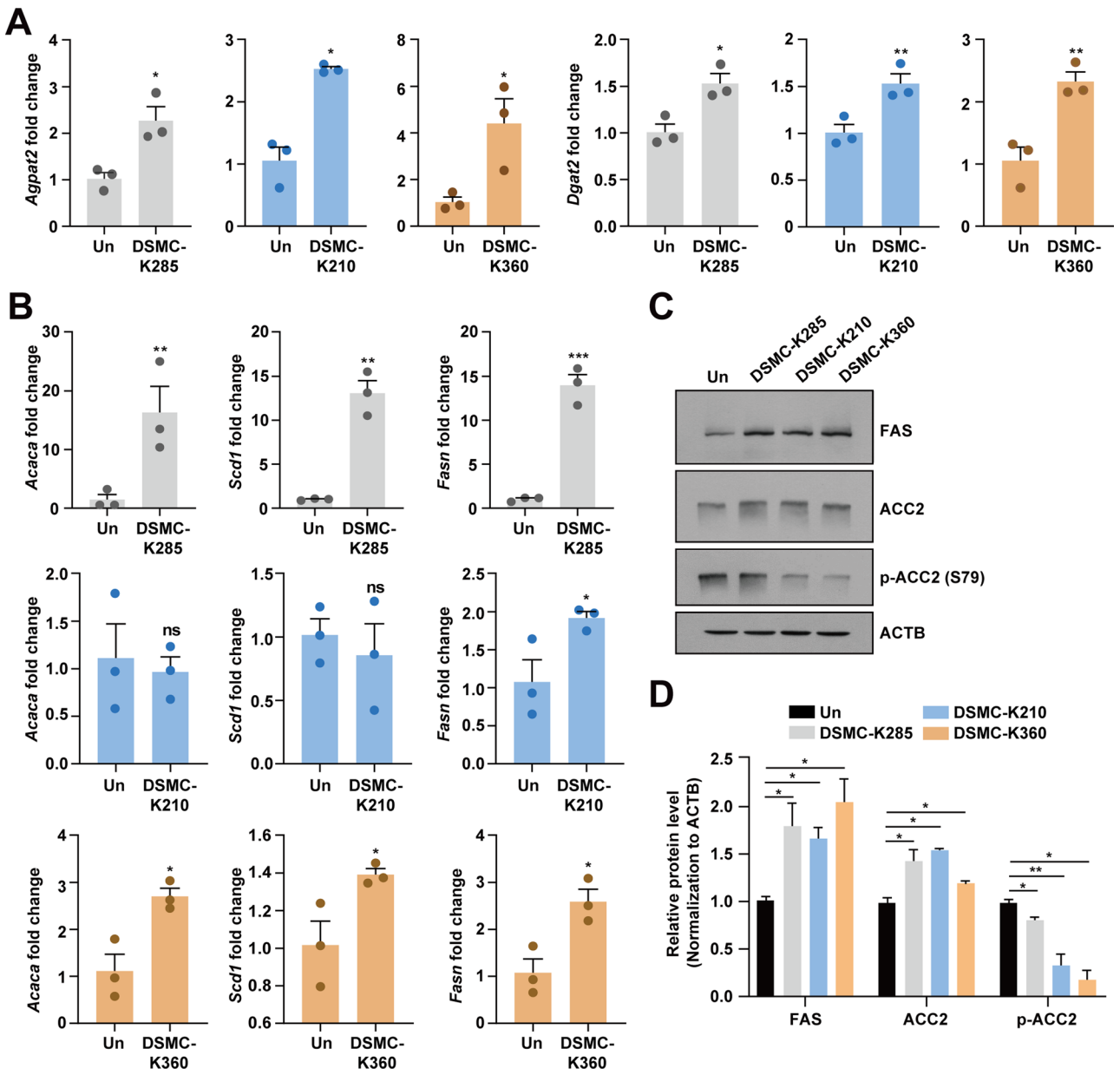

Fig. 2 HvKp infections alter lipid metabolism in RAW264.7 cells. **A**, **B** RAW264.7 cells were infected with hvKp strains (MOI 40) for 2 h. The mRNA levels of genes related to triglyceride synthesis (**A**) and fatty acid synthesis (**B**) were measured using qRT-PCR. **C**, **D** RAW264.7 cells were infected with hvKp strains (MOI 40) for 1 h. **C** Expression levels of proteins related to lipid metabolism (FAS, ACC2, and p-ACC2) in hvKp infections were determined via immunoblotting. **D** For quantitative analysis, bands were evaluated densitometrically using ImageJ analyzer software and normalized to ACTB density. Data are expressed as the mean ± standard deviation of three independent experiments. Un, uninfected; ns, not significant; LDs, lipid droplets. $*P<0.05$, $**P<0.01$, and $***P<0.001$ according to analysis of variance

Inhibiting LDs formation contributes to the survival of hvkp-infected mice

To further investigate the role of LDs formation during hvKp infection, we injected A922500 into mice and infected them with DSMC-K285. As shown in Fig. 6A, DGAT1 inhibition using A922500 decreased mortality compared with that of uninjected mice. In addition, A922500-injected mice did not exhibit significant differences in body weight compared with the control group, whereas uninjected mice showed a gradual decrease (Fig. 6B). As lipogenesis inhibitors suppress the intracellular survival of hvKp, we evaluated the effects of A922500 on antimicrobial responses in mice. Similar to RAW264.7 cells, we administrated A922500 by intraperitoneal (i.p.; Fig. 6C) or intranasal (i.n.; Fig. 6D) injection and infected C57BL/6 mice with DSMC-K285. We observed

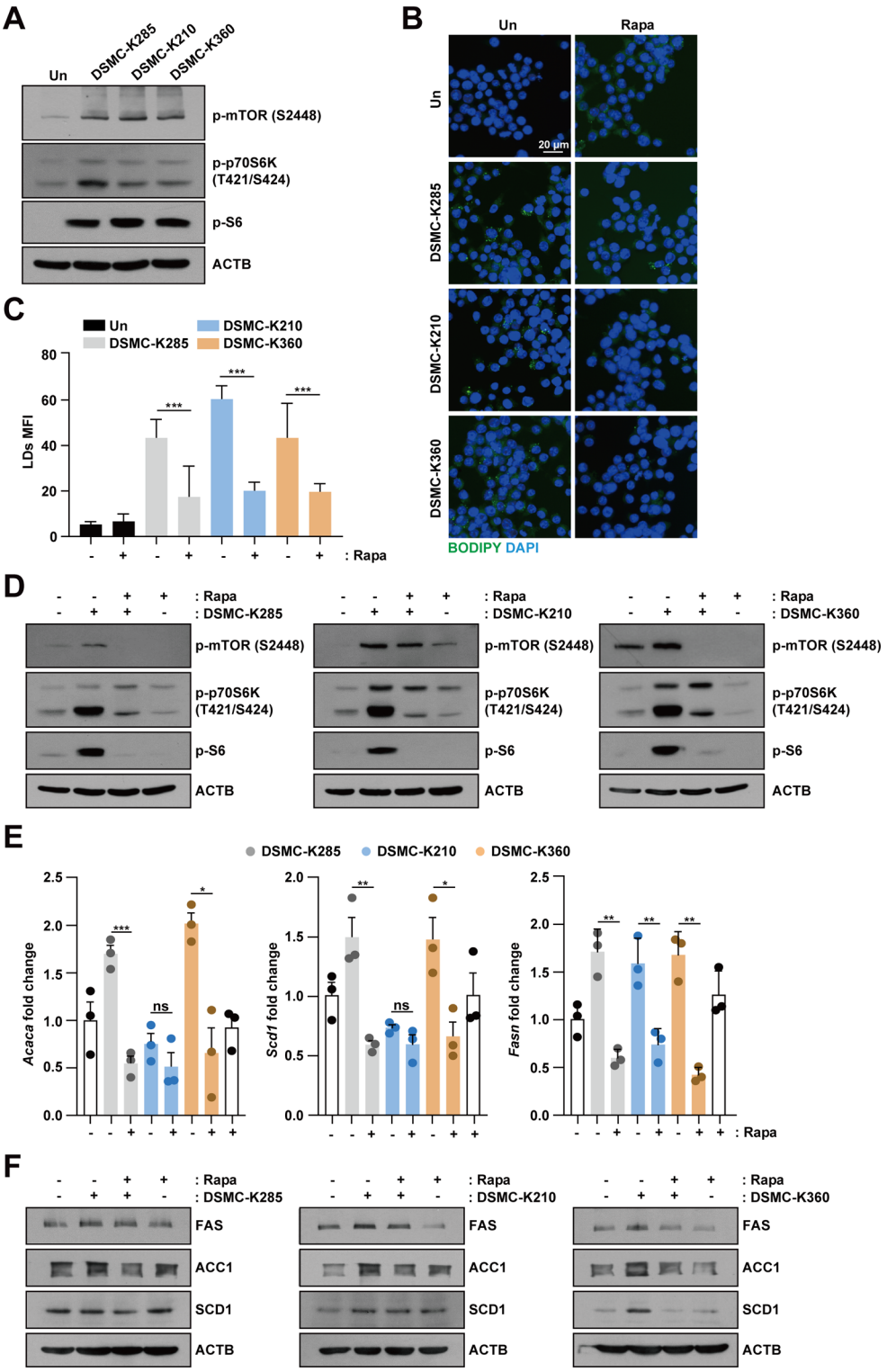

Fig. 3 The mTOR pathway is involved in LDs formation during hvKp infections. **A** RAW264.7 cells were infected with hvKp strains (MOI 40). After incubation for 1 h, the cells were lysed and subjected to immunoblotting using antibodies against phosphorylated mTOR, p70S6K, and S6. **B**, **C** RAW264.7 cells were incubated with or without rapamycin (200 nM) for 30 min and then infected with hvKp strains (MOI 40) for 4 h. **B** Cells were stained with BODIPY 493/503 (green) and DAPI (for nuclei). Scale bar, 20 μm. **C** Quantified mean fluorescent intensity (MFI) of the BODIPY signal based on independent fields of view for each group. **D** RAW264.7 cells were incubated with or without rapamycin (200 nM) for 30 min and then infected with hvKp strains (MOI 40) for 1 h. Proteins were detected using immunoblotting. **E**, **F** RAW264.7 cells were incubated with or without rapamycin (200 nM) for 30 min and then infected with hvKp strains (MOI 40) for 4 h. **E** The mRNA expression levels were determined using qRT-PCR. **F** Cells were lysed and subjected to immunoblotting using antibodies against FAS, ACC1, SCD1, and ACTB. Data are expressed as the mean ± standard deviation of the three independent experiments. Un, uninfected; ns, not significant; Rapa, rapamycin; mTOR, mammalian target of rapamycin; LDs, lipid droplets. $^{*}P < 0.05$, $^{**}P < 0.01$, and $^{***}P < 0.001$ according to analysis of variance

decreased viability of DSMC-K285 in the lungs, liver, and spleen following A922500 administration (Fig. 6C, D). Pathological changes in the various tissues were detected using H&E staining (Fig. 6E). Administration of A922500 reduced inflammatory cell infiltration, organized fibrin, edema, and inflamed areas, while the uninjected group showed severe pathological changes in the lungs. Moreover, neutrophils infiltration and the percentage of white pulp/red pulp ratio decreased in the A922500-injected livers and spleens, respectively. (Fig. 6E). Consistent with the in vitro results, we confirmed a decrease in the expression mRNA levels of *Tnfa* and *Il6*, and in TNF-α production in

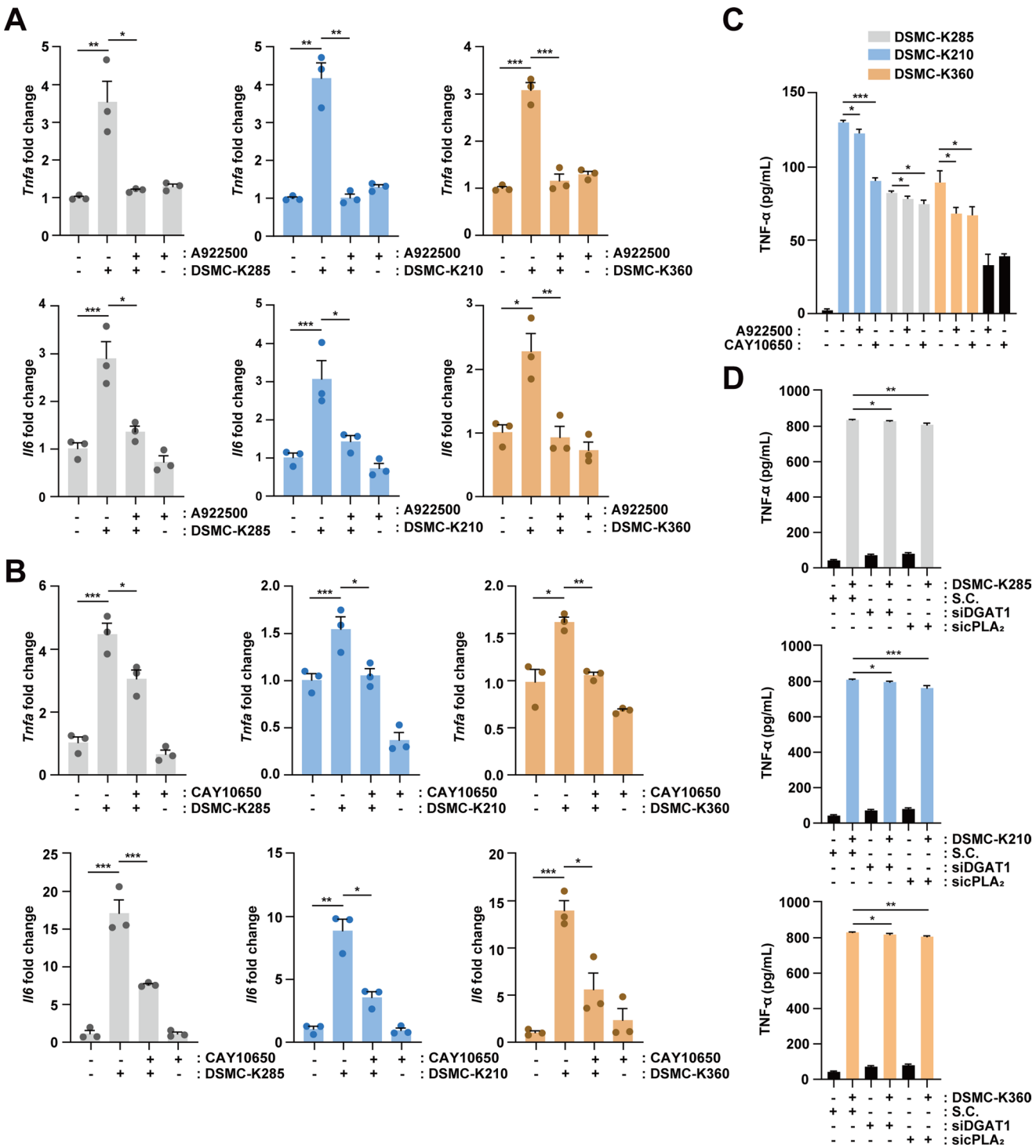

Fig. 4 LDs formation contributes to proinflammatory cytokine production during hvKp infections. **A**, **B** RAW264.7 cells were incubated with or without A922500 (10 μM; **A**) or CAY10650 (15 nM; **B**) for 1 h and then infected with hvKp strains (MOI 40) for 2 h. The mRNA expression levels of *Tnfa* and *Il6* were measured using qRT-PCR. **C** RAW264.7 cells were incubated with or without A922500 (10 μM) or CAY10650 (15 nM) for 1 h and then infected with hvKp strains (MOI 40) for 4 h. TNF-α levels were determined using ELISA. **D** RAW264.7 cells were transfected with siRNA specific for DGAT1 (siDGAT1), $cPLA_2$ ($sicPLA_2$), or a non-specific scrambled siRNA (S.C.). At 24 h after transfection, cells were infected with hvKp strains (MOI 40) for 4 h. Supernatants were then assessed by ELISA for TNF-α levels. Data are expressed as the mean ± standard deviation of three independent experiments. TNF, tumor necrosis factor; siRNA, small interfering RNA. $^{*}P < 0.05$, $^{**}P < 0.01$, and $^{***}P < 0.001$ according to analysis of variance

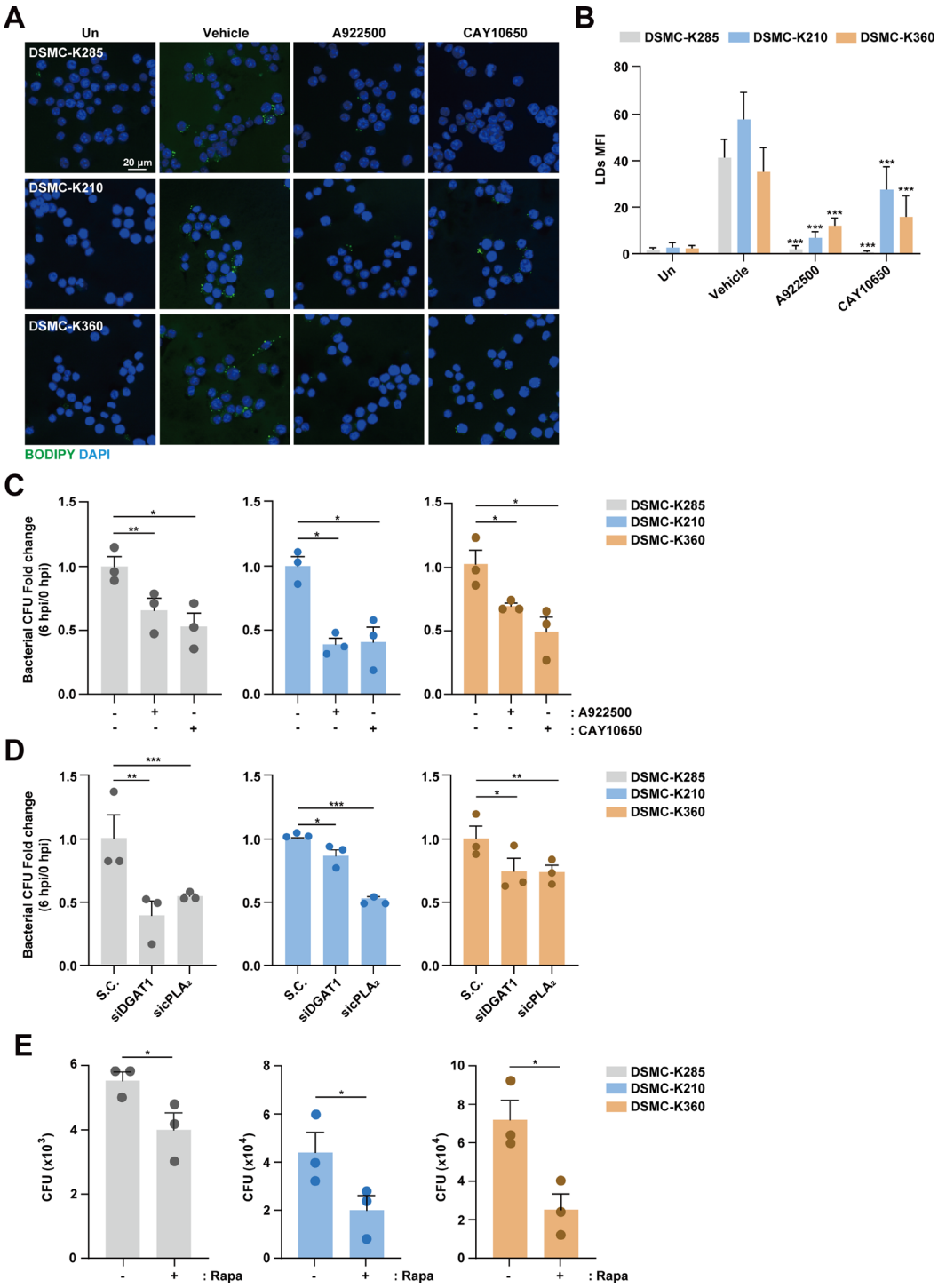

Fig. 5 Inhibiting LDs formation and knocking down of lipogenesis regulators promotes antimicrobial responses during hvKp infections. **A**, **B** RAW264.7 cells were pretreated with A922500 (10 μM) or CAY10650 (15 nM) for 1 h. Cells were then infected with hvKp strains (MOI 40) for 4 h. **A** Representative confocal images of LDs and nuclei were stained with BODIPY 493/503 (Green) and DAPI (Blue), respectively. Scale bar, 20 μm. **B** BODIPY 493/503 area quantification. **C** RAW264.7 cells were pretreated with A922500 (10 μM) or CAY10650 (15 nM) for 1 h, then infected with hvKp strains (MOI 40) for 6 h. Intracellular survival of hvKp was determined using colony forming units (CFU) assay. **D** RAW264.7 cells were transfected with siRNA against S.C., DGAT1, or $cPLA_2$ for 24 h and infected with the hvKp strains for 6 h. Intracellular survival of hvKp assessed by CFU assay. **E** RAW264.7 cells were pretreated with rapamycin (200 nM) for 30 min, followed by hvKp strain (MOI 40) infection for 6 h. Macrophage bacterial loads were detected using CFU assay. Data are expressed as the mean ± standard deviation of three independent experiments. Un, uninfected; LDs, lipid droplets; Rapa, rapamycin; hpi, hours post infection. $^{*}P < 0.05$, $^{**}P < 0.01$, and $^{***}P < 0.001$ according to analysis of variance

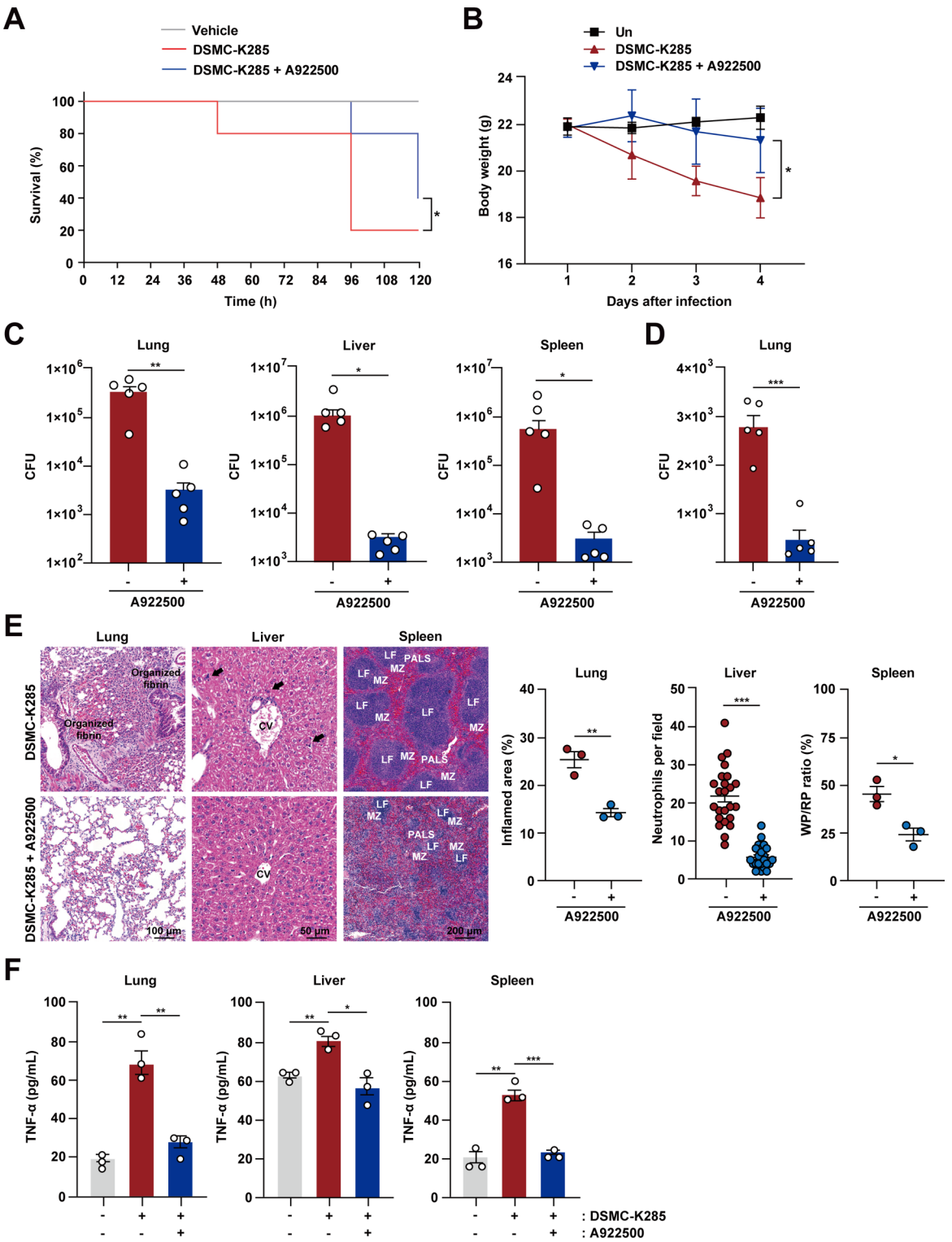

the tissues of the A922500-injected group (Supplementary Fig. 5A, B; Fig. 6F). These results confirm that inhibition of LDs formation plays an essential role in antimicrobial host defense against hvKp infections.

Discussion

De novo lipogenesis is an anabolic process that generates fatty acids from acetyl-CoA, which are utilized to produce TGs via the lipid remodeling pathway; excess lipids are

Fig. 6 A922500 treatment modulates antimicrobial responses in hvKp-infected mice. **A**, **B** C57BL/6 mice were i.p. infected with DSMC-K285 (1×10^3 CFU) and treated with A922500 (3 mg/kg) a day before infection. After 24 h of inoculation, the animals were euthanized. (**A**) Survival rates and (**B**) body weight of mice were recorded from Day 0 to 7. Data represent the mean ± standard deviation of three independent experiments ($n=5$ animals/group). **C-F** C57BL/6 mice were i.p. (**C**) or i.n. (**D**) infected with DSMC-K285 (1×10^3 CFU) and treated with A922500 (3 mg/kg) a day before infection. After 24 h of inoculation, the animals were euthanized. **C** In vivo bacterial loads in the lung, liver, and spleen tissues. **D** In vivo bacterial loads in the lung tissues. **E** Mice were injected with PBS or A922500 (i.p., 3 mg/kg) before DSMC-K285 (i.n., 1×10^3 CFU) infection. Representative H&E-stained images from lung, liver, and spleen tissues at 48 h (left). Black arrows indicate infiltrated neutrophils. Scale bars, 200 μm, 100 μm, and 50 μm. Morphometric estimation (right). **F** TNF-α levels were determined in the lung, liver, and spleen tissues using ELISA. Data represent the mean ± standard deviation of three independent experiments. Log-rank (Mantel-Cox) test is used to measure the significance. Un, uninfected; MZ, marginal zone; LF, lymphoid follicle; PALS, periarteriolar lymphoid sheath; WP, white pulp; RP, red pulp; CV, central vein. $^*P<0.05$, $^{**}P<0.01$, and $^{***}P<0.001$ according to analysis of variance

stored in LDs. LDs are organelles composed of a phospholipid monolayer and produce energy from stored lipids when required. Increasing evidence has revealed that LDs play critical roles in cellular processes, including lipid metabolism, cell signaling, immune responses, energy homeostasis, and membrane trafficking [25]. Thus, LDs regulation is closely related to the pathogenesis of many human diseases, such as diabetes, cancer, and obesity [26]. Recently, many studies have suggested that multiple intracellular pathogens target host LDs to survive within cells and obtain energy [27]. In mouse peritoneal macrophages, an *M. bovis* bacillus Calmette-Guérin infection has been found to result in LDs biogenesis and prostaglandin E2 production by toll-like receptor 2-PPARγ [28]. In particular, viruses replicate within cells using materials from the host; thus, many studies have reported on the role of LDs during viral infection [29]. For example, LDs accumulation is induced by herpes simplex virus 1 and Zika virus infections in primary immortalized astrocytes, whereas LDs upregulation upon viral infection enhances type-I and III interferon production, decreasing viral replication [30]. However, the role of intracellular LDs in host immune responses and host-pathogen interactions during hvKp infection is largely unknown. Our data demonstrated that infection with the three clinical hvKp strains leads to the upregulation of TGs synthesis and expression of lipogenic genes/proteins, resulting in LDs formation in the murine macrophage cell line. These results suggest that hvKp infection reprograms the host lipid metabolism.

As mTOR senses nutrients, growth factors, amino acids, and stress, the mTOR signaling pathway plays a vital role in cellular processes, including protein synthesis, mitochondrial biogenesis, autophagy, lipid biogenesis, and cell growth [23]. In macrophages, adipose-derived mesenchymal stromal cell-conditioned medium promotes LDs biogenesis via AKT/mTOR-PPARγ signaling [17]. Therefore, mTOR inhibitor rapamycin or PPARγ inhibitor GW9662 have been found to reduce LDs biogenesis [17]. In addition, the inhibition of mTOR by rapamycin decreases LDs in U937-derived foam cells [31]. We found that the mTOR-p70S6K-S6 signaling pathway was involved in LDs formation during hvKp infections. When the macrophages were treated with rapamycin, hvKp-induced LDs biogenesis and the expression of lipogenic genes and proteins decreased. Furthermore, rapamycin treatment affected the intracellular survival of hvKp in macrophages. Our results regarding mTOR pathway activation during hvKp infections in murine macrophages reveal the critical role of rapamycin in host defense and LDs biogenesis.

Additionally, Suelen et al. demonstrated increased LDs accumulation in the monocytes of patients with coronavirus disease 2019. Using A922500, they showed that LDs upregulation is required for the replication of severe acute respiratory syndrome coronavirus 2 replication [32]. Moreover, Zika virus infections induce LDs accumulation in neural cells, and in vivo viral loads are inhibited by A922500 treatment [33]. In addition, LDs inhibition using A922500 and the $cPLA_2$ inhibitor CAY10650 has been found to significantly decrease *S. Typhimurium* survival [15]. Therefore, we examined the effects of LDs inhibition on intracellular survival during hvKp infections. We found that treatment with A922500 or CAY10650 decreased the bacterial loads in murine macrophages.

Shuofeng et al. showed that siRNA knockdown of DGAT1 decreased severe acute respiratory syndrome coronavirus 2 replication in pulmonary Calu-3 cells [34]. Moreover, Eva et al. confirmed that DGAT1 activity is required for hepatitis C virus particle assembly using a DGAT1-targeting short hairpin RNA system [35]. However, studies on the role and importance of DGAT1 using genetic inhibition in bacterial infections are lacking. In addition, $cPLA_2$ is essential in the inflammatory response, where it produces arachidonic acid, which is then metabolized to produce proinflammatory molecules such as prostaglandins and leukotrienes [36]. During *Listeria monocytogenes* infection, $cPLA_2$ activation leads to arachidonic acid production, but unlike other infections, it results in reduced TNF-α production, indicating pathogen-specific immune response regulation [37]. $cPLA_2\alpha$ and $cPLA_2\gamma$ are activated in human macrophages upon infection with Mtb, leading to increased arachidonic acid release and TNF-α production, which triggers apoptosis of infected cells [38]. While there are many studies on $cPLA_2$ regulating the inflammatory response, research on its role in controlling intracellular bacterial survival during bacterial infections is still lacking. Importantly, our data showed that not only the pharmacological lipogenesis inhibitors but also the genetic inhibition of DGAT1 and $cPLA_2$ using siRNA reduced proinflammatory cytokine production and bacterial loads in macrophages.

To verify whether there is a decrease in the bacterial count within mice, we established an in vivo model of the hvKp infection. Since the clinical strains originate from a liver abscess, we infected the bacteria through i.p. injection. In agreement with in vitro data, we observed enhanced animal survival and decreased bacterial loads in the lungs, liver, and spleen in the A922500-injected group. In addition, greater body weight loss was observed in hvKp-infected mice, whereas A922500-injected mice were indistinguishable from control mice. These results strongly suggest that LDs play a crucial role in the host defense mechanisms against hvKp infections. As hvKp infections produce proinflammatory cytokines and induce a cytokine storm, causing a high mortality rate, regulating inflammation in host cells is important [9, 39, 40]. In addition, LDs inhibition has been observed to decrease inflammatory cytokine production in macrophages [24]; increased LDs levels result in excessive inflammation during *S. uberis* infections [14]. Therefore, we revealed the role of LDs in regulating inflammation during hvKp infections. Inhibition of LDs using inhibitors reduced hvKp-induced inflammatory cytokines, suggesting that the regulation of LDs biogenesis plays a role in host defense against hvKp infection. In mice, administering A922500 also inhibited hvKp infection-induced proinflammatory cytokine production. These results are consistent with those observed in vitro.

However, further studies are required to identify the bacterial effectors that alter host lipid metabolism and the mechanism by which lipogenesis inhibitors regulate inflammatory cytokine expression. In addition, as reported previously [41], clinical hvKp infections have shown different immune responses compared with those in cKp infections in murine macrophages. Therefore, a comparison of the altered host lipid metabolism during hvKp and cKp infections is required. Our study has several limitations should be highlighted. First, we lack knowledge of which effectors of hvKp can regulate changes in lipid metabolism within macrophages. Second, the study lacks an explanation of the mechanisms by which lipogenesis inhibitors regulate inflammatory mediators and bactericidal effects.

In summary, we highlighted the molecular mechanism of LDs biogenesis and the role of LDs in immune responses during clinical hvKp infections. Importantly, the present study has demonstrated that lipogenesis inhibitors show potent antimicrobial activities during hvKp infections. In particular, A922500 contributes to antimicrobial host defenses and inflammatory responses in vivo. Our data suggest that regulating LDs biogenesis is a potential therapeutic strategy, and A922500 may act as a promising candidate to treat hvKp infections by orchestrating multiple immune responses.

Supplementary Information The online version contains supplementary material available at https://doi.org/10.1007/s00430-024-00807-x.

Acknowledgements This work was supported by a National Research Foundation of Korea (NRF) Sejong Science fellowship (NRF-2022R1C1C2010228) and by NRF grants funded by the Korea government [MSIP] (NRF-2020R1F1A1070470 and RS-2023-00255021). We thank Dr. Eun-Jin Park (Chungnam National University College of Medicine) for experimental supports.

Author contributions H.-J.J. performed the experiments, analyzed the data, and wrote the manuscript. H.A.K. provided clinical hvKp strains and information. M.H. and J.Y.L. collected clinical hvKp strains and discussed the results. Y.J.K. supported mouse work. S.-I.S. supported analytical tools and reagents. E.-K.J. supported analytical tools, analyzed data, and mouse work. W.-K.B. and J.K.K. designed and supervised the study. All authors contributed to the article and approved the submitted version.

Data availability No datasets were generated or analysed during the current study.

Declarations

Competing interests The authors declare no competing interests.

References

1. Russo TA, Marr CA (2019) Hypervirulent *Klebsiella pneumoniae*. Clin Microbiol Rev 32(3)
2. Shon AS, Bajwa RP, Russo TA (2013) Hypervirulent (hypermucoviscous) *Klebsiella pneumoniae*: a new and dangerous breed. Virulence 4(2):107–118
3. Gu D, Dong N, Zheng Z, Lin D, Huang M, Wang L et al (2018) A fatal outbreak of ST11 carbapenem-resistant hypervirulent *Klebsiella pneumoniae* in a Chinese hospital: a molecular epidemiological study. Lancet Infect Dis 18(1):37–46
4. Long D, Zhu LL, Du FL, Xiang TX, Wan LG, Wei DD et al (2019) Phenotypical profile and global transcriptomic profile of Hypervirulent *Klebsiella pneumoniae* due to carbapenemase-encoding plasmid acquisition. BMC Genomics 20(1):480
5. Xu Q, Yang X, Chan EWC, Chen S (2021) The hypermucoviscosity of hypervirulent *K. pneumoniae* confers the ability to evade neutrophil-mediated phagocytosis. Virulence 12(1):2050–9
6. Russo TA, Olson R, Macdonald U, Metzger D, Maltese LM, Drake EJ et al (2014) Aerobactin mediates virulence and account for increased siderophore production under iron-limiting conditions by hypervirulent (hypermucoviscous) *Klebsiella pneumoniae.* Infect Immun 82(6):2356–67

7. Mina SA, Zhu G, Fanian M, Chen S, Yang G (2024) Exploring reduced macrophage cell toxicity of hypervirulent *Klebsiella pneumoniae* compared to classical Klebsiella pneumoniae. Microbiol Res 278:127515
8. Liu C, Guo J (2019) Hypervirulent *Klebsiella pneumoniae* (hypermucoviscous and aerobactin positive) infection over 6 years in the elderly in China: antimicrobial resistance patterns, molecular epidemiology and risk factor. Ann Clin Microbiol Antimicrob 18(1):4
9. Du P, Zhang Y, Chen C (2018) Emegece of carbapenemresistnt hypevirulent *Klebsiella pneumoniae*. Lancet Infect Dis 18(1):23–4
10. Arrese EL, Saudale FZ, Soulages JL (2014) Lipid droplets as Signaling platforms linking Metabolic and Cellular functions. Lipid Insights 7:7–16
11. den Brok MH, Raaijmakers TK, Collado-Camps E, Adema GJ (2018) Lipid droplets as Immune modulators in myeloid cells. Trends Immunol 39(5):380–392
12. Bozza PT, Bakker-Abreu I, Navarro-Xavier RA, Bandeira-Melo C (2011) Lipid body function in eicosanoid synthesis: an update. Prostaglandins Leukot Essent Fat Acids 85(5):205–213
13. Shim D, Kim H, Shin SJ (2020) *Mycobacterium tuberculosis* infection-driven foamy macrophages and their implications in tuberculosis control as targets for host-directed therapy. Front Immunol 11:910
14. Wan Z, Fu S, Wang Z, Xu Y, Zhou Y, Lin X et al (2022) FABP4-mediated lipid droplet formation in *Streptococcus uberis*-infected macrophages supports host defence. Vet Res 53(1):90
15. Pereira-Dutra KSE, Rajao FS, Ferraro-Moreira MA, Goltara-Gomes F, Cunha-Fernandes TC T et al (2022) Lipid droplet accumulation occurs early following *Salmonella* infection and contributes to intracellular bacterial survival and replication. Mol Microbiol 117(2):293–306
16. Nicolaou G, Goodall AH, Erridge C (2012) Diverse bacteria promote macrophage foam cell formation via toll-like receptor-dependent lipid body biosynthesis. J Atheroscler Thromb 19(2):137–148
17. Souza-Moreira L, Soares VC, Dias S, Bozza PT (2019) Adipose-derived mesenchymal stromal cells modulate lipid metabolism and lipid Droplet Biogenesis via AKT/mTOR -PPARgamma Signalling in macrophages. Sci Rep 9(1):20304
18. Hu X, Binns D, Reese ML (2017) The coccidian parasites *Toxoplasma* and *Neospora* dysregulate mammalian lipid droplet biogenesis. J Biol Chem 292(26):11009–11020
19. Peterson TR, Sengupta SS, Harris TE, Carmack AE, Kang SA, Balderas E et al (2011) mTOR complex 1 regulates lipin 1 localization to control the SREBP pathway. Cell 146(3):408–420
20. Franklin R, Cockerill MA, Wikler J, Alder MN, Dudley GM, Eliopoulos et al (2012) Mary Jane Ferraro Methods for Dilution Antimicrobial Susceptibility Tests for Bacteria That Grow Aerobically; Approved Standard—Ninth Edition. 9 ed. Clinical and Laboratory Standards Institute 32(2)
21. Compain F, Babosan A, Brisse S, Genel N, Audo J, Ailloud F et al (2014) Multiplex PCR for detection of seven virulence factors and K1/K2 capsular serotypes of *Klebsiella pneumoniae*. J Clin Microbiol 52(12):4377–4380
22. Laplante M, Sabatini DM (2009) An emerging role of mTOR in lipid biosynthesis. Curr Biol 19(22):R1046–R1052
23. Caron A, Richard D, Laplante M (2015) The roles of mTOR complexes in lipid metabolism. Annu Rev Nutr 35:321–348
24. Castoldi A, Monteiro LB, van Teijlingen Bakker N, Sanin DE, Rana N, Corrado M et al (2020) Triacylglycerol synthesis enhances macrophage inflammatory function. Nat Commun 11(1):4107
25. Walther TC, Farese RV (2012) Lipid droplets and cellular lipid metabolism. Annu Rev Biochem 81:687–714
26. Krahmer N, Farese RV Jr, Walther TC (2013) Balancing the fat: lipid droplets and human disease. EMBO Mol Med 5(7):973–983
27. Libbing CL, McDevitt AR, Azcueta RP, Ahila A, Mulye M (2019) Lipid droplets: a significant but understudied contributor of Host(-)Bacterial interactions. Cells 8(4):354
28. Almeida PE, Silva AR, Maya-Monteiro CM, Torocsik D, D'Avila H, Dezso B et al (2009) *Mycobacterium bovis* bacillus Calmette-Guerin infection induces TLR2-dependent peroxisome proliferator-activated receptor gamma expression and activation: functions in inflammation, lipid metabolism, and pathogenesis. J Immunol 183(2):1337–1345
29. Monson EA, Trenerry AM, Laws JL, Mackenzie JM, Helbig KJ (2021) Lipid droplets and lipid mediators in viral infection and immunity. FEMS Microbiol Rev 45(4)
30. Monson EA, Crosse KM, Duan M, Chen W, O'shea RD, Wakim LM et al (2021) Intracellular lipid droplet accumulation occurs early following viral infection and is required for an efficient interferon response. Nat Commun 12(1):4303
31. Zheng H, Fu Y, Huang Y, Zheng X, Yu W, Wang W (2017) mTOR signaling promotes foam cell formation and inhibits foam cell egress through suppressing the SIRT1 signaling pathway. Mol Med Rep 16(3):3315–3323
32. Dias SSG, Soares VC, Ferreira AC, Sacramento CQ, Fintelman-Rodrigues N, Temerozo JR et al (2020) Lipid droplets fuel SARS-CoV-2 replication and production of inflammatory mediators. PLoS Pathog 16(12):e1009127
33. Dias SSG, Cunha-Fernandes T, Souza-Moreira L, Soares VC, Lima GB, Azevedo-Quintanilha IG et al (2023) Metabolic reprogramming and lipid droplets are involved in Zika virus replication in neural cells. J Neuroinflammation 20(1):61
34. Yuan S, Yan B, Cao J, Ye ZW, Liang R, Tang K et al (2021) SARS-CoV-2 exploits host DGAT and ADRP for efficient replication. Cell Discov 7(1):100
35. Herker E, Harris C, Hernandez C, Carpentier A, Kaehlcke K, Rosenberg AR et al (2010) Efficient hepatitis C virus particle formation requires diacylglycerol acyltransferase-1. Nat Med 16(11):1295–1298
36. Chakraborti S (2003) Phospholipase A(2) isoforms: a perspective. Cell Signal 15(7):637–665
37. Noor S, Goldfine H, Tucker DE, Suram S, Lenz LL, Akira et al (2008) Activation of cytosolic phospholipase A2alpha in resident peritoneal macrophages by *Listeria monocytogenes* involves listeriolysin O and TLR2. J Biol Chem 283(8):4744–4755
38. Duan L, Gan H, Arm J, Remold HG (2001) Cytosolic phospholipase A2 participates with TNF-alpha in the induction of apoptosis of human macrophages infected with *Mycobacterium tuberculosis* H37Ra. J Immunol 166(12):7469–7476
39. Liu D, Chen Z, Yuan Y, Jing H, Zou J, Zhang X et al (2020) Innate Immune Effectors Play Essential Roles in Acute Respiratory Infection Caused by *Klebsiella pneumoniae*. J Immunol Res 2020:5291714
40. Peng W, Wu Y, Lu R, Zheng Y, Chen J, Pan P (2022) Successful treatment of acute respiratory distress syndrome caused by hypervirulent *Klebsiella pneumoniae* with extracorporeal membrane oxygenation and continuous renal replacement therapy: a case report and literature review. Front Med (Lausanne) 9:936927
41. Kim JK, Jung HJ, Hyun M, Lee JY, Park JH, Suh SI et al (2023) Resistance of hypervirulent *Klebsiella pneumoniae* to cathepsin B-mediated pyroptosis in murine macrophages. Front Immunol 14:1207121